

# Critical current calculations for long 0- $\pi$ Josephson junctions

I. Tornes and D. Stroud<sup>a</sup>

Department of Physics, Ohio State University, Columbus, OH 43210, USA

Received 14 April 2007 / Received in final form 2 September 2007

Published online 15 November 2007 – © EDP Sciences, Società Italiana di Fisica, Springer-Verlag 2007

**Abstract.** A zigzag boundary between a  $d_{x^2-y^2}$  and an  $s$ -wave superconductor is believed to behave like a long Josephson junction with alternating sections of 0 and  $\pi$  symmetry. We calculate the field-dependent critical current of such a junction, using a simple model. The calculation involves discretizing the partial differential equation for the phase difference across a long 0- $\pi$  junction. In this form, the equations describe a hybrid ladder of inductively coupled small 0 and  $\pi$  resistively and capacitively shunted Josephson junctions (RCSJ's). The calculated critical current density  $J_c(H_a)$  is maximum at non-zero applied magnetic field  $H_a$ , and depends strongly on the ratio of Josephson penetration depth  $\lambda_J$  to facet length  $L_f$ . If  $\lambda_J/L_f \gg 1$  and the number of facets is large, there is a broad range of  $H_a$  where  $J_c(H_a)$  is less than 2% of the maximum critical current density of a long 0 junction. All of these features are in qualitative agreement with recent experiments. In the limit  $\lambda_J/L_f \rightarrow \infty$ , our model reduces to a previously-obtained analytical superposition result for  $J_c(H_a)$ . In the same limit, we also obtain an analytical expression for the effective field-dependent quality factor  $Q_J(H_a)$ , finding that  $Q_J(H_a) \propto \sqrt{J_c(H_a)}$ . We suggest that measuring the field-dependence of  $Q_J(H_a)$  would provide further evidence that this RCSJ model applies to a long 0- $\pi$  junction between a  $d$ -wave and an  $s$ -wave superconductor.

**PACS.** 74.50.+r Tunneling phenomena; point contacts, weak links, Josephson effects – 74.81.Fa Josephson junction arrays and wire networks – 74.20.Rp Pairing symmetries (other than  $s$ -wave)

## 1 Introduction

Most hole-doped cuprate-based high-temperature superconductors are believed to be characterized by a  $d_{x^2-y^2}$  order parameter. Such an order parameter leads to many measurable consequences, but perhaps the most dramatic are due to so-called  $\pi$  junctions between a  $d_{x^2-y^2}$  superconductor and either a conventional,  $s$ -wave superconductor or another  $d_{x^2-y^2}$  superconductor. These  $\pi$  junctions can be detected by phase-sensitive symmetry measurements [1]. In a  $\pi$  junction, the Josephson current  $I$  and the gauge-invariant phase difference  $\gamma$  across the junction are related by  $I = I_c \sin(\gamma + \pi)$ [2], where  $I_c > 0$  is the junction critical current. By contrast, a conventional 0 junction satisfies  $I = I_c \sin \gamma$ . When a Josephson loop is formed by a suitable arrangement of  $d$ -wave and  $s$ -wave superconductors, the current-voltage (IV) characteristics differ dramatically from those found when only  $s$ -wave superconductors are involved. Such phase-sensitive experiments have provided some of the most persuasive evidence that the high- $T_c$  superconductors indeed have a  $d_{x^2-y^2}$  superconductor order parameter.

Recently, the  $d$ -wave nature of the order parameter was further confirmed by measurement of the IV characteris-

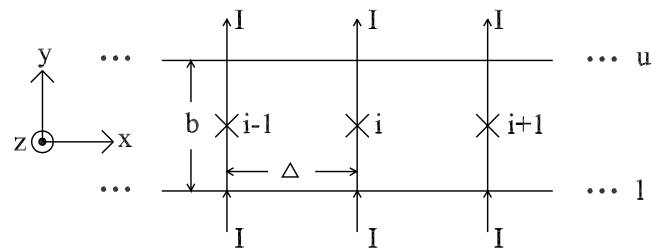


**Fig. 1.** Schematic view of Josephson ladder used in present calculations. The ladder has open boundary conditions;  $u$  and  $l$  represent the upper and lower edges of the ladder. A uniform current density  $J$  per unit length is applied in the  $\hat{y}$  direction. This corresponds to a current  $I = J\Delta$  applied across each rung in the ladder. An external magnetic field  $\mathbf{H}_a$  is applied in the  $\hat{z}$  direction.

tics of long “zigzag” junctions connecting two superconductors: a cuprate superconductor with an order parameter of  $d_{x^2-y^2}$  symmetry, and Nb, an  $s$ -wave superconductor [3,4]. In the experiments of reference [3], the cuprate

<sup>a</sup> e-mail: stroud@mps.ohio-state.edu

superconductor was  $\text{YBa}_2\text{Cu}_3\text{O}_{7-x}$  (YBCO), while in reference [4],  $\text{Nd}_{2-x}\text{Ce}_x\text{CuO}_{4-y}$  (NCCO) was used. The geometry of the zigzag junction is shown in Figure 1 of reference [3], which also shows the expected orientation of the order parameter lobes on each side of the junction. In this configuration, the zigzag junction is expected to consist of alternating sections of 0 and  $\pi$  junctions, as shown in that figure. In the experiments, the IV characteristics of this zigzag junction were measured in the presence of an external magnetic field applied parallel to the facets of the superconductor, i.e. perpendicular to the plane of the figure. The response of the junctions was, indeed, found to be consistent with the expected  $d_{x^2-y^2}$  symmetry of YBCO and NCCO.

In this paper, we use a simple numerical model to calculate the critical current density  $J_c(H_a)$  of a long 0- $\pi$  Josephson junction as a function of the applied magnetic field  $H_a$ . One of our goals is to obtain a general picture of how  $J_c(H_a)$  behaves in this model as a function of the variables  $\lambda_J/L_f$  and  $N_f$ , where  $L_f$  is the length of one facet of the junction  $\lambda_J$  is the Josephson penetration depth, and  $N_f$  is the number of facets. A second goal is to see how well our simple model agrees with the experimental results [3,4] for 0- $\pi$  zigzag junctions. A final goal is to connect our approach to other treatments of long 0- $\pi$  junctions. We find that, in the limit  $\lambda_J/L_f \gg 1$ , the model reduces to a generalized superposition approximation previously used to treat such junctions [4,5]. However, even in that limit, we obtain new information, namely, an analytical expression for the field-dependent quality factor  $Q_J(H_a)$  of the long junction.

A characteristic feature of a one-dimensional array of alternating 0 and  $\pi$  junctions is the occurrence of half-integer flux quanta, in the region where the 0 and  $\pi$  junctions join. Many features of these half-integer flux quanta have been studied analytically and numerically by Goldobin et al. [6,7], in zero applied magnetic field. Our approach is basically a discretized version of this model, but extended to a finite magnetic field. In particular, our model does contain the half-quanta which are responsible for some of the observed experimental features.

Qualitatively, our calculated IV characteristics agree fairly well with experiment. For example, the measured field-dependent critical current  $I_c(H_a)$  of the zigzag junction found to be symmetric in  $H_a$ , with a principal maximum at nonzero  $H_a$ . This behavior is in contrast to a long 0 (or long  $\pi$ ) junction, which will have a maximum  $I_c(H_a)$  at  $H_a = 0$ . Our model reproduces these features. We also obtain the result that, when  $\lambda_J/L_f \gg 1$  and the long junction has many facets, there is a broad range of  $H_a$  where  $J_c(H_a)$  is only  $\sim 1$ -2% of the maximum critical current density. In the experiments of [3,4], it is found that  $J_c(H_a)$  is very small over a wide range of  $H_a$ .

The remainder of this paper is arranged as follows. In Section 2, we describe our simple model. The numerical results obtained from this model are given in Section 3. In Section 4, we show that the model reduces to a generalized superposition approximation in the limit  $\lambda_J/L_f \rightarrow \infty$ , and we obtain the effective quality factor  $Q_J(H_a)$  in the

same limit. Finally, we give a concluding discussion in Section 5.

## 2 Formalism

We consider a long Josephson junction consisting of alternating 0 and  $\pi$  sections, or facets, as in the zigzag junctions studied experimentally. Let the length of one such facet be  $L_f$ , and let there be  $N_f$  such facets, so that the total junction length is  $L = N_f L_f$ . We use coordinates such that the alternating series of facets runs along the  $x$  axis, and the plates of the junction are normal to the  $y$  axis. In addition we assume that there is a uniform magnetic field  $\mathbf{H}_a = H_a \hat{\mathbf{z}}$  applied parallel to the junction plates.

The gauge-invariant phase  $\gamma(x, t)$  across the junction satisfies the following partial differential equation:

$$\gamma_{tt} = -\sin \gamma + \lambda_J^2 \gamma_{xx} + \frac{J}{J_{c0}} + \frac{1}{Q_J} \gamma_t - \pi \lambda_J^2 n_{xx}. \quad (1)$$

Equation (1) is equivalent to equation (1) of reference [7] in the case when  $H_a$  is uniform. In this equation, the subscripts  $x$  and  $t$  represent derivatives with respect to position  $x$  and a dimensionless time  $\omega_p t$ ,  $x$  being the coordinate along the junction.  $\lambda_J$  is the Josephson penetration depth and  $\omega_p$  is the Josephson plasma frequency,  $J$  is the driving current per unit length across the junction (assumed uniform), and  $J_{c0}$  is the critical current per unit length of a 0 junction at zero applied field ( $H_a = 0$ ). In terms of the junction parameters,  $\omega_p^2 = 2eJ_{c0}/(\hbar C)$  where  $C$  is the junction capacitance per unit length.  $Q_J = \omega_p C/G$  is the junction quality factor, and  $G \equiv 1/R$  is the normal shunt conductance of the junction per unit length. For a junction connecting two non-identical materials  $\lambda_J^{-2} = 8\pi e(\lambda_1 + \lambda_2 + d)\bar{J}_c/(\hbar c^2)$ [2], where  $\bar{J}_c$  is the critical current per unit area and  $\lambda_1$  and  $\lambda_2$  are the penetration depths of the materials on either side of the junction. Finally,  $n(x)$  indicates whether the point  $x$  lies within a 0 or a  $\pi$  facet:  $n(x) = 0$  in a 0 facet and  $n(x) = 1$  in a  $\pi$  facet.

In this formulation, the applied magnetic field does not appear explicitly in the differential equation; instead, it appears as a boundary condition:  $\gamma(L, t) - \gamma(0, t) = 2\pi H_a d_{\text{eff}} L/\Phi_0 + [n(L) - n(0)]\pi$ , where  $\Phi_0 = hc/(2e)$  is the flux quantum.

The gauge-invariant phase can also be expressed as

$$\phi(x, t) = \gamma(x, t) - \frac{2\pi}{\Phi_0} \int_i^j \mathbf{A}_a \cdot d\mathbf{l} - \pi n(x), \quad (2)$$

where  $\mathbf{A}_a$  is the vector potential corresponding to the applied field  $\mathbf{H}_a$ , and the integral runs between the plates of the junction in the  $y$  direction. It is convenient to work in a gauge such that  $\mathbf{A}_a = H_a x \hat{\mathbf{y}}$ , so that  $(2\pi/\Phi_0) \int \mathbf{A} \cdot d\mathbf{l} = 2\pi H_a d_{\text{eff}} x/\Phi_0$ .  $d_{\text{eff}}$  is the effective thickness of the junction, which we may express in terms of  $\lambda_1$ ,  $\lambda_2$ , and the actual Josephson barrier thickness  $d$  as  $d_{\text{eff}} = d + \lambda_1 + \lambda_2$ .

The equation of motion for the new variable  $\phi(x, t)$  across the junction may now be written as

$$\phi_{tt} = -\sin\left[\phi + \frac{2\pi}{\Phi_0}H_a d_{\text{eff}}x + \pi n(x)\right] + \lambda_J^2 \phi_{xx} + \frac{J}{J_{c0}} - \frac{1}{Q_J} \dot{\phi}, \quad (3)$$

with the boundary conditions  $\phi_x(0, t) = \phi_x(L, t) = 0$ . For numerical purposes, equation (3) is generally more convenient than equation (1), because, in the latter,  $n(x)$  is only piecewise continuous, and hence  $n_{xx}$  is the sum of derivatives of Dirac delta functions. Note also that  $H_a$  appears explicitly in equation (3), whereas in equation (1) it appears only as a boundary condition.

In order to treat equation (3) numerically, it is convenient to discretize it in space, by breaking the long junction into  $N$  small segments, or “mini-junctions,” each of length  $\Delta$  ( $L = N\Delta$ ). We also assume that each  $0$  or  $\pi$  facet is divided into an integer number  $N_p$  of such mini-junctions, so that  $L_f = N_p\Delta$  and thus  $N_p N_f = N$ . Denoting the phase difference across the  $i$ th such junction by  $\phi_i$ , we obtain a collection of  $N$  coupled ordinary differential equations. Except for  $i = 1$  and  $i = N$ , these may be written

$$\ddot{\phi}_i = -\sin(\phi_i + 2\pi i f/N_p + n_i\pi) + \frac{\lambda_J^2}{\Delta^2}(\phi_{i+1} - 2\phi_i + \phi_{i-1}) + \frac{J}{J_{c0}} - \frac{1}{Q_J} \dot{\phi}_i. \quad (4)$$

Here we have introduced the frustration  $f = H_a L_f d_{\text{eff}}/\Phi_0$ , defined as the flux per facet in units of  $\Phi_0$ . For  $i = 1$  and  $i = N$ , the second term on the right hand side of equation (4) must be modified, and the equation of motion becomes

$$\ddot{\phi}_i = -\sin(\phi_i + 2\pi i f/N_p + n_i\pi) + \frac{\lambda_J^2}{\Delta^2}(\phi_{i+1} - \phi_i) + \frac{J}{J_{c0}}\phi_i - \frac{1}{Q_J} \dot{\phi}_i, \quad (5)$$

and

$$\ddot{\phi}_i = -\sin(\phi_i + 2\pi i f/N_p + n_i\pi) + \frac{\lambda_J^2}{\Delta^2}(\phi_{i-1} - \phi_i) + \frac{J}{J_{c0}}\phi_i - \frac{1}{Q_J} \dot{\phi}_i \quad (6)$$

for  $i = 1$  and  $i = N$  respectively.

Equations (4–6) describe a *hybrid Josephson ladder*, consisting of  $N$  mini-junctions inductively coupled together in parallel, and driven by an applied uniform dc current. The geometry is shown schematically in Figure 1. The driving current is in the  $y$  direction and the field is in the  $z$  direction. We use the phrase “hybrid ladder” to distinguish this system from the more conventional Josephson ladders, which have junctions on both the rungs and the edges [8]. The limit of physical interest, however, is the continuum limit, i.e.,  $N_p \rightarrow \infty$ .

### 3 Numerical results

Before describing our results, we make some qualitative remarks about the relation between our model and the

zigzag junction used in experiments [3,4]. Although our  $0-\pi$  junction is straight, it does have one crucial feature in common with the zigzag junction, namely, intrinsic frustration, even at zero applied magnetic field. We define the frustration  $\tilde{f}_i$  of the plaquette lying between the  $i$ th and  $(i + 1)$ th mini-junction as

$$\tilde{f}_i = \frac{f}{N_p} \quad (7)$$

if both junctions are either  $0$  junctions or  $\pi$  junctions, and

$$\tilde{f}_i = \frac{f}{N_p} + \frac{1}{2} \quad (8)$$

if one is a  $0$  junction and the other is a  $\pi$  junction. If  $\tilde{f}_i$  is an integer, the energies of all the bonds making up the plaquette can be simultaneously minimized, and the plaquette is unfrustrated. If  $\tilde{f}_i$  is non-integer, the bond energies cannot all be simultaneously minimized, and the actual bond configuration is a compromise among these; in this case, the plaquette is frustrated.

The effects of frustration are easily understood if  $N_p = 1$ . Then the long  $0-\pi$  junction is represented by a hybrid ladder having alternating sections of  $0$  and  $\pi$  junctions. Thus, according to the above definition, the ladder is frustrated ( $\tilde{f}_i \neq 0$ ) at all fields, including  $H_a = 0$ , with the exception of  $f = 1/2$ , i.e., one-half quantum of flux per facet. At this field, the ladder is unfrustrated, and we expect that the critical current per facet will be maximum. Moreover, that maximum (per facet) should equal the critical current of a single  $0$  facet at  $H_a = 0$ , namely  $L_f J_{c0}$ . At all other fields, the critical current will be smaller than that maximum value.

If  $N_p > 1$ , the ladder has some residual frustration even at  $f = 1/2$ . For example, at  $N_p = 2$  and  $f = 1/2$ , each plaquette has  $\tilde{f}_i = 3/4$ . Thus, although we expect the critical current still to be maximum at  $f = 1/2$ , that maximum will be smaller than  $L_f J_{c0}$ . Since the physical system is really in the continuum limit ( $N_p \rightarrow \infty$ ), we generally expect a critical current which is smaller than  $L_f J_{c0}$  even at the optimum value of  $f = 1/2$ . This expectation is borne out by our calculations below.

Although the  $0-\pi$  ladder configuration of Figure 1 does have the frustration characteristic of a zigzag junction, it still differs geometrically from the one shown in Figure 1 of reference [3], even in the continuum limit, because the zigzag junction is not straight. The bends in the zigzag junction will introduce some pinning which is absent from our model, and therefore will probably lead to slightly different IV characteristics than those produced by the model of Figure 1, possibly more closely resembling experiment.

We turn now to our calculations. We have solved equations (4–6) for  $0-\pi$  junctions made of various numbers of facets  $N_f$ , numbers  $N_p$  of mini-junctions per facet, facet lengths  $L_f$ , Josephson penetration depths  $\lambda_J$ , and applied fields  $f$ . In all cases, we obtain the solutions to the coupled differential equations using a standard fourth order Runge-Kutta technique. Our goal is to obtain the critical

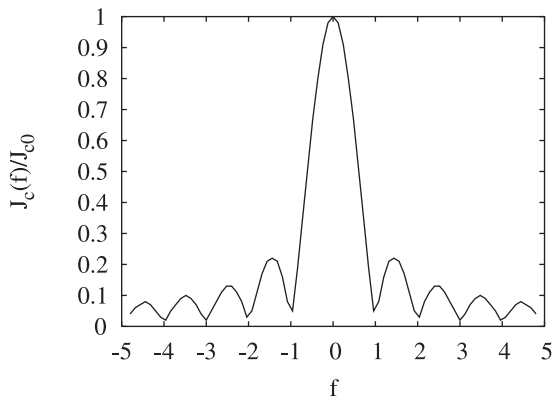


**Fig. 2.** Calculated critical current per unit length  $J_c(f)$  for a 0 junction of length  $L_f$ , plotted as function of the flux  $f$  through the facet.  $f$  is given in units of a flux quantum  $\Phi_0 = hc/(2e)$ . The facet is represented as a hybrid ladder of 120 small 0 junctions, as described in the text. The Josephson penetration depth  $\lambda_J = 1.3L_f$  and the quality factor  $Q_J = 6.0$ .  $J_{c0}$  is the critical current per unit length of a 0 junction at zero applied field.

current of a long 0- $\pi$  junction as a function of these parameters, as well as of the Josephson penetration depth  $\lambda_J$ . In principle, we are interested in the continuum limit, corresponding to  $N_p \rightarrow \infty$ . Any effects arising from finite  $N_p$  will be absent from a real 0- $\pi$  junction, and are therefore artifacts of the finite discretization length  $\Delta$ . In general, we expect that  $\phi(x)$  will vary only on a length scale of  $\lambda_J$ . Therefore, if  $L_f \ll \lambda_J$ , we should not need a large  $N_p$  to approach this continuum limit. Our numerical results support this expectation, as we discuss below.

We first consider a single 0 junction in an external field  $f$ . If  $\lambda_J > L$ , then the critical current per unit length,  $J_c(f)$ , should exhibit a Fraunhofer-like pattern [2]. Figure 2 of reference [3], which shows their measured  $I_c(H_a)$  for a single long 0 junction, clearly exhibits this Fraunhofer pattern.

To calculate this pattern in our model, we apply a specified field  $f$  to the junction, then ramp up the external driving current density  $J$  until a non-zero voltage is recorded, giving  $J_c(f)$ .  $f$  is then increased and the process is repeated. Since the value of  $Q_J$  is not explicitly given in the experimental papers [3,4], we arbitrarily choose  $Q_J = 6$  in all our calculations. This value will lead to hysteretic IV characteristics for at least some  $f$ , as in the experiments.

In Figure 2, we show our calculated  $J_c(f)/J_{c0}$  for a hybrid Josephson ladder of 120 rungs with all 0 junctions, open boundary conditions, a penetration depth  $\lambda_J = 1.3L$ , and  $Q_J = 6$ . Figure 2 shows that our ladder configuration behaves similarly to the long 0 junction studied experimentally (Fig. 2 of Ref. [3]), and hence, our discretization of the long junction into 120 mini-junctions is on a sufficiently fine scale to produce the Fraunhofer pattern seen experimentally. Comparing Figure 2 to the experimental figure, we see that  $f \sim 1.44$  is equivalent to  $H_a \sim 1.1 \mu\text{T}$ . Since all our IV characteristics are obtained

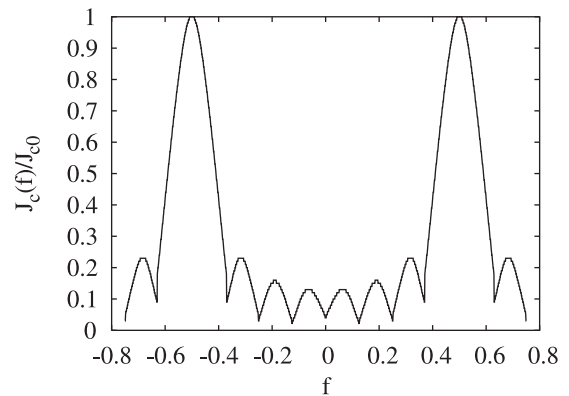


**Fig. 3.** Critical current per unit length  $J_c(f)$ , in units of  $J_{c0}$ , plotted as a function of the magnetic flux per facet  $f$ , for an eight-facet junction of alternating 0 and  $\pi$  facets, open boundary conditions,  $\lambda_J = 2.6L_f$  and  $Q_J = 6.0$ . The junction is modeled as a hybrid Josephson ladder with one mini-junction per facet, as described in the text.

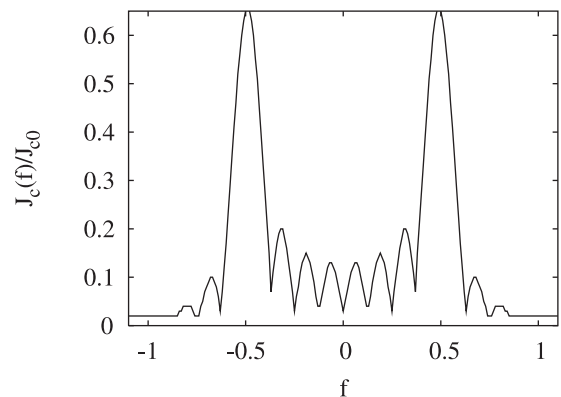


**Fig. 4.** Same as in Figure 3, but with five mini-junctions per facet.

on the increasing current branch, we have not checked for the expected hysteresis seen in the experiment.

According to conventional theory [2], the Fraunhofer pattern in a long Josephson junction results from simple superposition:  $J_c(H_a) = J_{c0} |\sin(\pi\Phi/\Phi_0)/(\pi\Phi/\Phi_0)|$ , where  $\Phi$  is the flux through the junction area  $L(d + 2\lambda)$ . This result is obtained [2] by assuming that the phase  $\phi(x)$  [Eq. (2)] is independent of  $x$ , or equivalently, that  $\phi_i$  is independent of  $i$  [Eqs. (4-6)]. Although, for this particular  $\lambda_J/L_f$ , we obtain numerical results very close to this asymptotic form, our approach is more general than simple superposition. In particular, we do *not* assume that the  $\phi_i$ 's are all the same. Instead, the  $\phi_i$ 's, at any applied current density  $J$ , are always the values which satisfy the coupled differential equations. Thus, in principle, our approach gives a different result from superposition, even for this simple case. This point is discussed further below.

In Figures 3, 4, and 5, we show the calculated  $J_c(f)$  (obtained on the increasing current branch) for a ladder

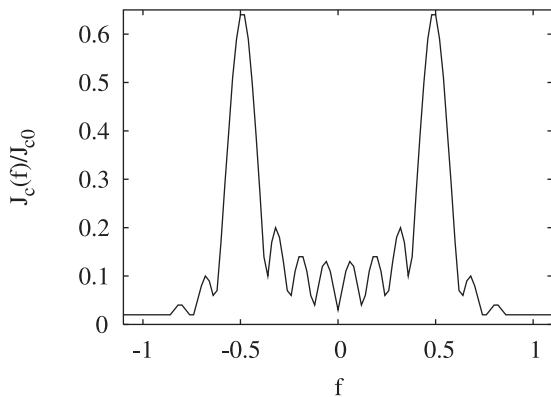


**Fig. 5.** Same as in Figure 3, but with ten mini-junctions per facet.

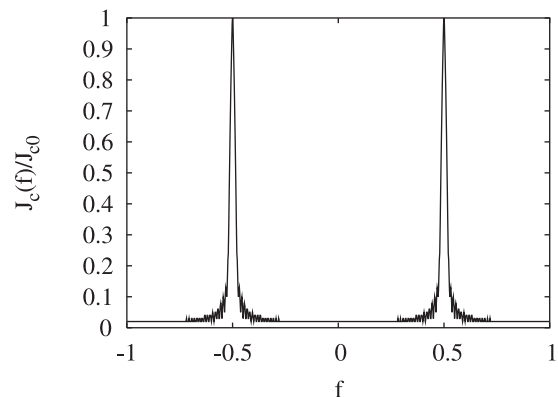


**Fig. 6.** Same as in Figure 3, but with 80 facets, one mini-junction per facet, and  $\lambda_J = 13L_f$ .

consisting of eight alternating  $0$  and  $\pi$  facets, open boundary conditions,  $Q_J = 6$ , and  $\lambda_J = 2.6L_f$ , but with each facet divided into one, five, and ten mini-junctions, respectively. In all three cases, our calculations show  $J_c(f)$  to be symmetric around  $f = 0$ , with maxima at  $f = \pm 1/2$ . In the case  $\Delta = L_f$ ,  $J_c(f = \pm 1/2)$  equals the zero-field critical current of a pure  $0$  junction, but for  $\Delta = L_f/5$  and  $\Delta = L_f/10$ ,  $J_c(\pm 1/2)$  is smaller than this value. This behavior can be understood as follows. For  $\Delta = L_f$ , the eight-facet  $0-\pi$  ladder becomes perfectly unfrustrated at  $f = \pm 1/2$ , and thus should behave like the  $f = 0$  ladder of  $0$  junctions. However, in the other two cases, there is still some residual frustration at  $f = \pm 1/2$ , and hence  $J_c(\pm 1/2)$  is reduced.

$J_c(\pm 1/2)$  has approximately the same magnitude in Figures 4 and 5, suggesting that the  $N_p = 5$  case is already close to the asymptotic limit ( $\Delta \rightarrow 0$ ), at least for  $f = \pm 1/2$ . In general,  $J_c(f)$  has strong peaks at  $f = 1/2 + m$ , where  $m$  is an integer, but these peaks are unequal except for  $N_p = 1$ . From Figures 4 and 5, we see that the heights of the first *three* peaks in  $I_c(f)$  do not change when we go from  $N_p = 5$  to  $N_p = 10$ . This is once again a consequence of the fact that  $N_p = 10$  or even  $N_p = 5$  is close to the continuum limit for these values of  $f$  and  $N_f$ . The model calculations of Figures 4 and 5 are clearly more realistic than that with  $N_p = 1$ , because they allow  $\phi$  to vary *within* a single facet.

In Figure 3, but not Figures 4 and 5,  $J_c(f)$  is periodic with period unity. This periodicity is an artifact; it occurs because  $N_f = 1$  in Figure 3, which causes the equations of motion to be periodic with period unity. By contrast, this periodicity is absent if  $N_f > 1$ . If  $L_f = N_p\Delta$ , the equations of motion are periodic in  $f$  with period  $N_p$ . But since the physically relevant limit is  $N_p \rightarrow \infty$  or  $\Delta \rightarrow 0$ , this periodicity is also an artifact of the discretization.

Another notable feature of Figures 3–5 is that each shows exactly six secondary maxima between the two principal maxima in  $J_c(f)$ . These maxima occur at about the same values of  $f$  no matter how finely the facet is discretized. Moreover, they do not start to overlap as the number of mini-junctions is increased. The maxima can

be understood from a generalization of the Fraunhofer pattern described above to the case of  $N_f$  alternating  $0$  and  $\pi$  junctions. This generalization has been given in equation (3) of reference [4], and, using a slightly different derivation, in reference [5]. This generalized Fraunhofer pattern (not shown in the figure) agrees remarkably well with the numerically calculated  $J_c(f)$  our eight-facet junction. We believe the slight deviation is due to the fact that the phases within each facet, in our dynamical model, are obtained directly by solving the equations of motion for the long junction rather than by a superposition argument.

Finally, we comment on another feature of Figures 4 and 5, but not Figure 3, namely the existence of an approximate, but not exact, plateau in  $J_c(f)$ . In our numerical studies for these two ladder systems, we find that the smallest critical current density  $J_c(f)$  is in the range of 1% – 2% of the critical current density  $J_{c0}$  of a single facet. Moreover,  $J_c(f)$  remains in this range over a broad range of  $f$ . This range of values of 1% – 2% remains the same regardless of how small we make the incremental increases in the driving current. We believe that this approximate plateau can also be understood from the superposition argument mentioned above. More details of this approximate plateau are discussed below.

To further investigate the behavior of  $J_c(f)$  in a different range of the ratio  $\lambda_J/L_f$ , we have carried out additional calculations for a ladder of alternating  $0$  and  $\pi$  facets with  $Q_J = 6$ ,  $N_f = 80$ , and a ratio  $\lambda_J/L_f = 13$ , the latter two parameters being the same as in recent experiments [3]. We consider three cases:  $N_p = 1$ ,  $N_p = 2$ , and  $N_p = 4$ . The results of these calculations, shown in Figures 6, 7a and 7b, and 8, are quite different from those shown previously. Now, for almost all values of  $f$  between  $-0.5$  and  $0.5$ ,  $J_c(f) \sim 0.01 - 0.02J_{c0}$ . Very close to  $f = \pm 1/2$ ,  $J_c(f)$  increases slightly, and exactly at  $f = \pm 1/2$ ,  $J_c(f)/J_{c0} = 1$  in Figure 6. The behavior at  $f = \pm 1/2$  is consistent with expectations, since, for  $N_p = 1$  the ladder is unfrustrated at these values of  $f$ . If we consider  $N_p = 2$  and  $N_p = 4$ , but keep  $\lambda_J/L_f = 13$ , the positions of the peaks remain unchanged and their heights

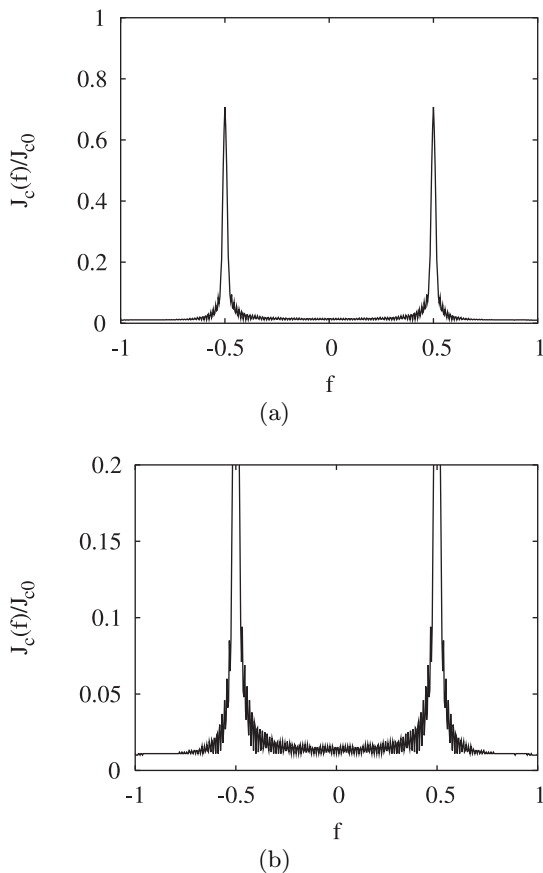


**Fig. 7.** (a) (top): Same as in Figure 6, but with two mini-junctions per facet. In contrast to Figure 6, we have incremented the current density in increments of  $0.001J_{c0}$  to calculate the critical current. With this fine scale, small oscillations in  $J_c(f)$  are clearly apparent in the “plateau” region, which is not perfectly flat. (b) (bottom): same as (a), except that we have magnified the vertical scale to make the oscillations more visible.

change in a predictable manner similar to that already found in Figures 3–5. In both figures, as in Figure 6, there are, as expected, strong peaks in  $J_c(f)$  at  $f = 1/2 + m$ , with  $m$  an integer. When  $N_p \geq 2$ , the peak heights are smaller than unity, as already expected from the results shown in Figures 4 and 5. The close resemblance between  $N_p = 2$  and  $N_p = 4$  suggests that the continuum limit is already approached by  $N_p = 4$ .

We have carried out many other calculations (not shown here) for other values of  $\lambda_J/\Delta$ . In general, we find that this approximate plateau occurs over the widest range of  $f$  when  $\lambda_J/\Delta \gg 1$  and when  $N_f \gg 1$ . Although the experiments [3] are not sensitive enough to measure  $J_c(f)$  in the range of  $0.01$ – $0.02J_{c0}$ , they do show that  $J_c(f) \sim 0$  over a broad range of  $f$ .

We have done various numerical checks to confirm that the plateau is not a numerical artifact. These checks are carried out primarily for the results of Figure 7. To carry out the checks, we have typically, for a given  $f$ , ramped

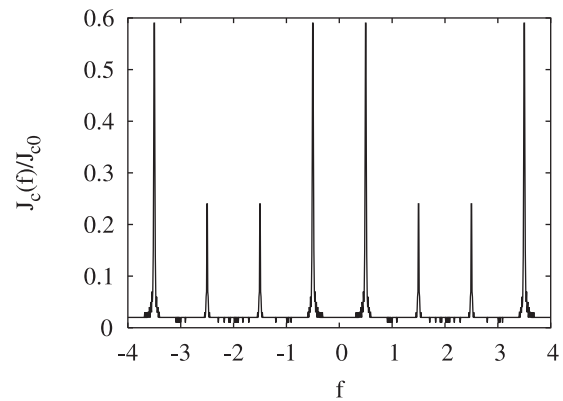


**Fig. 8.** Same as in Figure 6, but with four mini-junctions per facet. As in Figure 6, we increment the current density in intervals of  $0.01J_{c0}$ . At this resolution, most of the plateau region looks flat, but we expect that, if calculated with increments of  $0.001J_{c0}$  it would show oscillations as in Figure 7.

up  $J$  in units of  $0.001J_{c0}$ , where  $J_{c0}$  is the critical current density of a single facet, rather than  $0.01J_{c0}$  as in the calculations shown in the other figures. To compute  $J_c(f)$ , after ramping up  $J$ , we iterated the coupled Josephson equations for a dimensionless time  $\omega_p t = 300$ , then averaged the voltage over the next interval of 200.  $J_c(f)$  was taken as the value of  $J$  for which the time-averaged voltage, as determined in this way, first becomes non-zero. We then incremented  $f$  by  $0.01$ , reset  $J$  to zero, and again incremented the current density in steps of  $0.001J_{c0}$  to find the next  $J_c(f)$ . In this way, we found that the  $J_c(f)$  in the plateau region varies between about  $0.012J_{c0}$  and  $0.016J_{c0}$ .

The results of these calculations, for a ladder of 80 facets with two mini-junctions per facet, are shown in Figure 7a and 7b. Here, we see that  $J_c(f)$ , though small over a wide range of  $f$ , is not actually perfectly flat, as mentioned above, but instead has small-amplitude oscillations as a function of  $f$ . Note that, because of the amount of computer time needed to do these simulations in which the current is incremented by only  $0.001J_{c0}$  rather than  $0.01J_{c0}$ , we have done the small-increment calculations only in Figures 7a and 7b, and not Figures 6 and 8. As in all the other figures showing  $J_c(f)/J_{c0}$  versus  $f$ ,  $J_c(f)$  is taken to be that value of  $J$  above which the time-averaged voltage  $\langle V \rangle$  jumps up to its value on the resistive branch of the hysteretic current-voltage characteristic, i.e.  $\langle V \rangle = J_{c0}/G$ , where  $G$  is the shunt conductance per unit length. Clearly,  $J_c(f)$  is indeed non-zero on the plateau, and remains nonzero over a broad range of  $f$  whenever  $N_f$  is large enough.

We have also calculated  $J_c(f)$  using the simple superposition theory of references [4] and [5]. The results, shown in Figure 9, are remarkably similar to those in Figure 8. Thus, although our calculations are based on a numerical solution of the coupled Josephson equations appropriate to this geometry, the field-dependent critical current closely resembles that obtained by a simple superposition

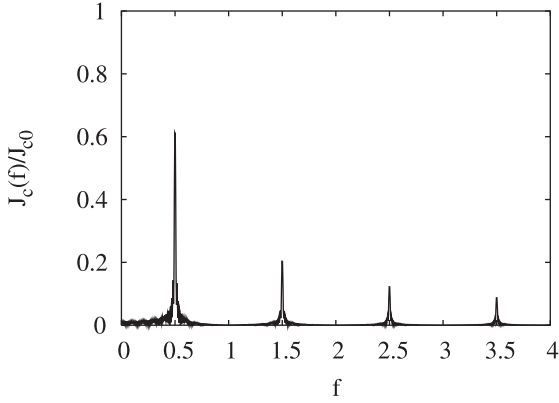


**Fig. 9.**  $J_c(f)/J_{c0}$  as obtained from the superposition approximation of references [4] and [5] for a long  $0-\pi$  junction having 80 facets.

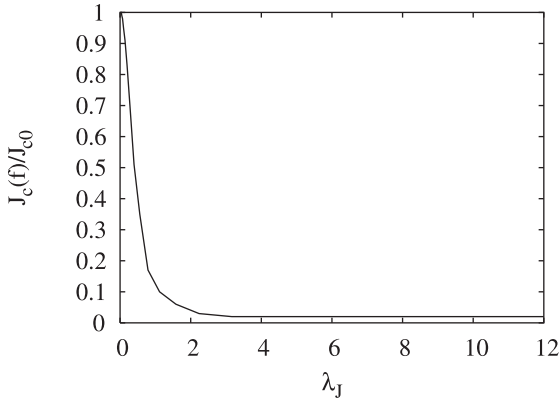


**Fig. 10.** Critical current per unit length  $J_c(f)$ , in units of  $J_{c0}$ , for  $f = 0$  and an 80-facet  $0-\pi$  junction modeled as in the text for  $f = 0$ , assuming one mini-junction per facet, and plotted as a function of  $\lambda_J/L_f$ .

theory. In particular, the heights of the first two sharp peaks in  $J_c(f)$  as calculated numerically, for  $f > 0$ , are similar to those obtained using the generalized superposition approximation.

Finally, to show explicitly how  $J_c(f)/J_{c0}$  depends on  $\lambda_J$ , we have calculated the critical current at *zero* applied field ( $f = 0$ ) for an alternating  $0-\pi$  ladder with 80 facets, each of length one junction ( $N_p = 1$ ), as a function of  $\lambda_J$ . The results are shown in Figure 10. The results of this figure are calculated incrementing  $J/J_{c0}$  by 0.01 for each value of  $\lambda_J$ . For very small  $\lambda_J$  the ladder just behaves like many uncoupled small junctions, and  $J_c(0) = J_{c0}$ . As  $\lambda_J$  increases,  $J_{c0}$  decreases, until  $\lambda_J \sim \sqrt{10}$ . For  $\lambda_J > \sqrt{10}$ ,  $J_c(0) \sim 0.02J_{c0}$ . Once again, this value is not exact, but fluctuates slightly with  $\lambda_J$ .

## 4 Generalized superposition limit

Since our results closely resemble the simple superposition theory (or “generalized Fraunhofer limit”), we have examined our equations of motion [Eqs. (4–6)] in an effort to understand when that model gives the superposition limit. First, we sum these equations to obtain an expression for  $(1/N)\sum_{i=1}^N \ddot{\phi}_i$ . With the definition  $\phi = (1/N)\sum_{i=1}^N \phi_i$ , and the use of several trigonometric identities, we finally obtain

$$\ddot{\phi} = -A \sin(\phi + \theta) + J/J_{c0} - \dot{\phi}/Q_J, \quad (9)$$

where

$$A = \sqrt{C^2 + S^2}, \quad (10)$$

$$\theta = \tan^{-1}(S/C), \quad (11)$$

$$C = \frac{1}{N} \sum_i \cos(2\pi i f/N_p + n_i \pi + \phi_i - \phi), \quad (12)$$

$$S = \frac{1}{N} \sum_i \sin(2\pi i f/N_p + n_i \pi + \phi_i - \phi). \quad (13)$$

The “superposition limit” is appropriate when the phase  $\phi_i$  is independent of  $i$ . We expect this to be true when  $\lambda_J \gg L_f$ , in which case  $\phi_i$  should vary little across the zigzag junction. In this limit,  $\phi_i - \phi = 0$ , both  $C$  and  $S$  are independent of  $\phi$ , and equation (9) just becomes the equation of motion for a single RCSJ with a field-dependent critical current and quality factor. Both of these can be obtained with the change of variables  $\psi = \phi + \theta$ , in terms of which equation (9) becomes

$$\ddot{\psi} = -A \sin(\psi) + J/J_{c0} - \dot{\psi}/Q_J. \quad (14)$$

With the further change of variables  $\tau' = \tau/\sqrt{A}$ , this last equation becomes

$$\ddot{\psi} = -\sin \psi + J/(AJ_{c0}) - \dot{\psi}/(\sqrt{A}Q_J). \quad (15)$$

Equation (15) describes a single Josephson junction with a critical current density

$$J_c^s(f) = AJ_{c0} \quad (16)$$

and quality factor

$$Q_J^s(f) = \sqrt{A}Q_J = Q_J \left( \frac{J_c(f)}{J_{c0}} \right)^{1/2}, \quad (17)$$

where the superscript denotes the superposition approximation.

To obtain the value of  $A$  (in the physically relevant continuum limit  $\Delta \rightarrow 0$ ), we rewrite  $C$  as  $C = \text{Lim}_{N \rightarrow \infty} (N\Delta)^{-1} \sum_{i=1}^N [\Delta \cos(2\pi i f/N_p + n_i \pi)]$  or, converting the sum to an integral,  $C = 1/(N_f L_f) \int_0^{N_f} L_f dx \cos[2\pi f x/L_f + n(x)\pi]$ . The integral

can be done analytically.  $S$  can be obtained in analogous fashion. The resulting expressions for  $C^2$  and  $S^2$ , and hence  $A = \sqrt{C^2 + S^2}$  and  $J_c^s(f) = AJ_{c0}$ , can be shown to reduce to that given in equation (3) of reference [4], namely (using our variables as defined earlier)

$$C^2 = \frac{1}{2\pi f} \left\{ \sum_{n=1}^{N_f} \sin[n(\pi - 2\pi f)] [1 - \cos(2\pi f)] - \sum_{n=1}^{N_f} \cos[n(\pi - 2\pi f)] \sin(2\pi f) \right\}^2 \quad (18)$$

and

$$S^2 = \frac{1}{2\pi f} \left\{ \sum_{n=1}^{N_f} \cos[n(\pi - 2\pi f)] [1 - \cos(2\pi f)] + \sum_{n=1}^{N_f} \sin[n(\pi - 2\pi f)] \sin(2\pi f) \right\}^2. \quad (19)$$

Thus, our approach does reduce, as it should, to simple superposition in the limit when the phases  $\phi_i$  are independent of  $i$ . We expect this limit to be appropriate when  $\lambda_J \gg L_f$ . We also obtain an additional piece of information in this limit, namely, the effective value of the junction quality factor  $Q_J^s(f)$ . Our result for this quality factor is not particularly surprising. The reason why the quality factor becomes smaller at certain fields is not that the local damping changes with field. Rather, it is because the critical current is reduced at certain magnetic fields by cancellation between different parts of the junction, leading to an increase in the *relative* dissipation in the junction at these fields. If  $\lambda_J/L_f$  is finite, the superposition approximation is not exact, because  $\phi_i$  will be dependent on  $i$ . In this case, we should expect deviations from its predictions for  $J_c(f)$ . These are, indeed, observed in our calculations (and shown explicitly in Fig. 10).

## 5 Discussion

We have presented a simple model for field-dependent critical current density  $J_c(H_a)$  of a long  $0-\pi$  junction. An important example of such a system is a zigzag junction connecting an  $s$ -wave superconductor and one with a  $d_{x^2-y^2}$  order parameter. We numerically solve for the IV characteristics of this junction by discretizing the equation of motion in space and time. The model gives, not only  $J_c(H_a)$ , but also (in principle) the full IV characteristics and its hysteretic behavior when the shunt resistivity is large.

In the limit  $\lambda_J \rightarrow \infty$ ,  $J_c(H_a)$  for our model reduces to that predicted by a generalized superposition model [3, 5]. However, our model is more general, because it applies for finite  $\lambda_J/L_f$  and hence accounts for the variation of the phase along the junction. Furthermore, even in the limit  $\lambda_J \rightarrow \infty$ , the model gives not only the analytical form for  $J_c(H_a)$ , as previously obtained in references [4]

and [5], but also a field-dependent effective quality factor  $Q_J(H_a)$ . The field-dependence of  $Q_J(H_a)$  is due to cancellation effects within the long  $0-\pi$  junction as a function of  $H_a$ , rather than any field-dependence of the assumed local damping within the junction.

Our numerical results qualitatively resemble the experiments on  $d$ - $s$  zigzag junctions [3, 4]. As in the experiment, we obtain a strong maximum in  $J_c(H_a)$  at a non-zero magnetic field, which is comparable in magnitude to its unfrustrated value,  $J_{c0}$ . Furthermore, our results, like the experimental ones, depend strongly on the ratio  $\lambda_J/L_f$ . Finally, for large  $\lambda_J/L_f$  and large numbers of facets  $N_f$ , we find that  $J_c(H_a)$  is very small over a broad range of magnetic field and in the range of 1–2% of  $J_{c0}$ . The experiments are not sensitive enough to measure such a small  $J_c(H_a)$  but they also show broad ranges of  $H_a$  where  $J_c(H_a)$  is very small. The origin of this large region of very small  $J_c(H_a)$  is undoubtedly the cancellation resulting from superimposing the currents from different parts of the long  $0-\pi$  junction, as implied by the superposition model. The experimental results appear to have some fine structure not present in our model. We do not know the origin of this fine structure, but speculate that it may be due to the bends in the zigzag junction, which are not included in the model.

Finally, we also comment briefly on the applicability of the RCSJ model to a junction connecting an  $s$ -wave superconductor to one with  $d_{x^2-y^2}$  symmetry. One possible concern is that, in the  $d$ -wave superconductor, since the energy gap vanishes at certain points in  $k$ -space, it is relatively easy for a current to excite quasiparticles and, therefore, possibly heat the superconductor. Therefore, if a fluxon moves through a long  $0-\pi$  junction, it might easily cause localized heating in the junction. If this heating occurs, it would tend to mask the RCSJ behavior of the long  $0-\pi$  junction. One might also ask how accurately the RCSJ model would describe the long junction, even without heating. Clearly, the RCSJ model is an idealized approximation of the real junction behavior. But the model seems to be a reasonable starting point for possible, more refined approaches. Moreover, the RCSJ behavior can potentially be tested, in the limit when the Josephson penetration depth  $\lambda_J$  is large compared to a facet length. Namely, in this limit, the RCSJ model implies that the effective junction quality factor  $Q_J(H_a)$  is proportional to the square root of the field-dependent critical current density  $J_c(H_a)$ . If experiments show this dependence, this would represent evidence that the RCSJ model is indeed applicable to a long  $0-\pi$  junction.

The present work suggests several questions which could be further studied in experiments. For example, it would be of interest to study  $0-\pi$  zigzag junction when  $\lambda_J/L_f$  is smaller than unity. In this range, we would expect substantial departures from the generalized superposition model, as suggested by Figure 10 for  $f = 0$ . In addition, it would be desirable to test the predicted dependence of  $Q_J(f)$  on  $f$  experimentally in the superposition limit. Since  $J_c(f)$  may be small over a broad range of  $f$ , equation (17) suggests that a long  $0-\pi$  junction would

behave as if overdamped at these values of  $f$  even if it is underdamped and hysteretic when  $J_c(f)$  is large. It would be of interest to test this hypothesis experimentally.

This work has been supported through NSF Grant DMR04-13395. Some of the calculations were carried out using the facilities of the Ohio Supercomputer Center, with the help of a grant of time.

## References

1. D.J. Van Harlingen, Rev. Mod. Phys. **67**, 515 (1995); C.C. Tsuei, J.R. Kirtley, Rev. Mod. Phys. **72**, 969 (2000), and references cited therein
2. See, for example, M. Tinkham, *Introduction to Superconductivity*, 2nd edn. (McGraw-Hill, New York, 1996)
3. Ariando, D. Darminto, H.J.H. Smilde, V. Leca, D.H.A. Blank, H. Rogalla, H. Hilgenkamp, Phys. Rev. Lett. **94**, 167001 (2005)
4. H.J.H. Smilde, Ariando, D.H.A. Blank, G.J. Gerritsma, H. Hilgenkamp, H. Rogalla, Phys. Rev. Lett. **88**, 057004 (2002)
5. R.G. Mints, V.G. Kogan, Phys. Rev. B **55**, 8682(R) (1997)
6. E. Goldobin, D. Koelle, R. Kleiner, Phys. Rev. B **66**, 100508(R) (2002)
7. E. Goldobin, D. Koelle, R. Kleiner, Phys. Rev. B **67**, 224515 (2003)
8. See, for example, S. Flach, M. Spicchi, J. Phys.: Cond. Mat. **11**, 321 (1999); P. Binder, D. Abraimov, A.V. Ustinov, S. Flach, Y. Zolotaryuk, Phys. Rev. Lett. **84**, 745 (2000); W.B. Yu, E.B. Harris, S.E. Hebboul, J.C. Garland, D. Stroud, Phys. Rev. **45**, 12624 (1992); M. Barahona, S.H. Strogatz, T.P. Orlando, Phys. Rev. B **57**, 1181 (1998); F. Falo, A.R. Bishop, P.S. Lomdahl, Phys. Rev. B **41**, 10983 (1990), and references cited therein